Nanoscience and Technology: An International Journal

ISSN Print: 2572-4258; ISSN Online: 2572-4266

Begell House, USA.

Accepted September 30th 2020

ENTROPY GENERATION IN MAGNETOHYDRODYNAMIC RADIATIVE NON-NEWTONIAN DISSIPATIVE CONVECTION FLOW FROM AN INCLINED PLANE: NUMERICAL STUDY

S. Abdul Gaffar[1]*, Khalil-Ur-Rehman[2], O. Anwar Bég[3], V. Ramachandra Prasad[4]

[1]Department of Mathematics, Salalah College of Technology, Salalah, Oman

[2]Department of Mathematics, Air University, PAF Complex E-9, Islamabad 44000, Pakistan

[3]Multi-Physical Engineering Sciences, Mechanical/Aeronautical Engineering, University of Salford, M54WT, UK.

[4]Department of Mathematics, School of Advanced Sciences, VIT University, Vellore, India

**** Corresponding Author: Email – abdulsgaffar0905@gmail.com***

ABSTRACT

A theoretical model is developed to study entropy generation in non-Newtonian magnetohydrodynamic thermal convection from an inclined plate as a simulation of electro-conductive polymer materials processing of relevance to automotive coating applications. High temperature invokes radiative effects which are analysed with the Rosseland diffusion flux approximation. The Jeffery's viscoelastic model is deployed to describe the non-Newtonian characteristics of the fluid and provides a good approximation for magnetic polymers, which constitutes a novelty of the present work. The normalized nonlinear boundary value problem is solved computationally with the Keller-Box implicit finite-difference technique. Extensive solutions for *velocity, surface temperature, skin friction and heat transfer rate* are visualized graphically for various thermophysical parameters. Validation is conducted with earlier published work for the case of a vertical plate in the absence of magnetic field, radiative flux and non-Newtonian effects. The dimensionless entropy generation is obtained via the reduced momentum and energy equations. Bejan number is generally decreased with greater values of Deborah number. Increasing magnetic field reduces entropy generation number whereas it enhances the Bejan number. Increasing Brinkman number (dissipation parameter) is found to enhance the entropy generation number whereas it suppresses the Bejan number.

KEYWORDS: *Viscoelastic fluid; Inclined plate; magnetohydrodynamics; thermal convection; thermal radiation; retardation time; Bejan number; Entropy generation number; Hartmann number; numerical solutions.*

NOMENCLATURE

B_0	*Constant imposed magnetic field*	$\boldsymbol{V}$	*Velocity vector*
Be	*Dimensionless Bejan number*	u, v	*Dimensionless velocity components in X and Y direction respectively*
Br	*Brinkmann number*	x	*Stream wise coordinate*
C_f	*Skin Friction Coefficient*	y	*Transverse coordinate*

c_p	*specific heat*		***Greek Symbols***
De	*Deborah Number*	α	*Thermal diffusivity*
f	*Dimensionless stream function*	β	*Coefficient of thermal expansion*
F	*Thermal radiation*	λ	*ratio of relaxation to retardation times*
g	*Gravitational acceleration*	λ_1	*retardation time*
Gr	*Thermal Grashof number*	η	*Non-dimensional transverse coordinate*
Ha	*Hartmann number*	σ	*Electric conductivity of the fluid*
k	*Thermal conductivity of the fluid*	θ	*Dimensionless temperature*
k^*	*Mean absorption coefficient*	ρ	*Fluid density*
M	*Magnetic parameter*	ξ	*dimensionless tangential coordinate*
N_G	*Entropy generation number*	ψ	*Non-dimensional stream function*
Nu	*Heat transfer coefficient (Local Nusselt number)*	σ^*	*Stefan-Boltzmann constant*
Pr	*Prandtl number*	μ	*Dynamic viscosity*
q_r	*Radiative heat flux*	ξ	*Non-dimensional tangential coordinate*
R	*Mixed convection parameter*	ν	*Kinematic viscosity*
Re	*Reynolds number*		***Subscripts***
S	*Cauchy stress tensor*	*w*	*Conditions on the wall*
T	*Fluid temperature*	∞	*Free stream condition*

1. INTRODUCTION

Transport phenomena from inclined surfaces arise in many applications in industry. These include fuel combustion [1], condensation systems [2], magnetic thin film deposition [3], geophysical debris flows [4], thermal coating [5] and geothermal heat transfer from oblique faults [6]. In materials processing systems, the use of an inclined plane allows thermal buoyancy force to be easily modified since it is proportional to the inclination angle. Materials manufacturing operations (e.g. plastic coating dynamics [7], gel and thin film systems [8]) also frequently feature non-Newtonian fluids. Rheology of the involved fluids significantly modifies momentum and heat transfer characteristics in such flows. In the context of thermoplastic sheet processing, Johnson [9] considered polymer flows on rigid inclines, viscoelastic film flows may become unstable due to fluid elasticity which is controlled by the Weissenberg number. Many rheological models have subsequently been deployed in recent years to study thermal and momentum boundary-layer flows from inclined surfaces. These studies have also utilized many advanced numerical methods which are required to accommodate the nonlinearity of such flows. Sui *et al.* [10] used the Ostwald-DeWaele power-law model and homotopy analysis method (HAM) to investigate thermal convection from a non-isothermal inclined surface with wall transpiration (lateral mass flux). They observed that thermal convection is suppressed with a reduction in inclination angle. Shamshuddin *et al.* [11] investigated time-dependent chemically-reacting micropolar double diffusive convection

from an inclined sheet with Ohmic dissipation using a perturbation method. They observed that the flow is strongly decelerated with greater inclination of the plate from the vertical case. Helal and Saif [12] employed a shooting numerical method to compute solutions for natural convection thermo-solutal boundary layer flow of pseudoplastic and dilatant fluids from a tilted plane in the presence of thermophoresis. Chinyoka *et al.* [13] analysed the unsteady non-isothermal gravity driven flow of a variable viscosity viscoelastic Oldroyd-B liquid along an inclined plane with convective cooling at the free surface. Among the many viscoelastic fluids available, the Jeffrey model [14] has emerged as a good approximation for polymer dynamics. This model features three constants, namely the zero shear-rate viscosity, ratio of relaxation and retardation time and the retardation time. It is appropriate for nonlinear viscoelastic effects for which the simpler inelastic models cannot be used. Jeffrey's model is obtained by adding a time derivative of the shear rate to the conventional Maxwell linear model. The convected Jeffrey model (Oldroyd model) also allows several other special cases to be obtained. When retardation time is neglected the original Maxwell model is retrieved. When the relaxation time is neglected then the case of a second order differential fluid is obtained for which the normal stress coefficient is zero. Finally, when both relaxation and retardation times are equivalent then the Newtonian fluid case is obtained. Jeffrey's model was used by Prasad *et al.* [15] to study steady-state thermal polymer coating flow of a plate in porous media. Gaffar *et al.* [16] investigated the non-isothermal and non-isolutal transport phenomena from a porous conical body using the Jeffrey model. These studies all showed how significant modifications are computed in heat, flow and species diffusion fields due to viscoelastic material behaviour.

In recent years thermal process engineers have embraced a new approach to optimize heat efficiency in the design of thermal systems, entropy generation minimization (EGM). This approach assists the engineer in identifying for example which manufacturing process is most efficient. It utilizes the second law of thermodynamics to build more sophisticated models of heat transfer which allow a deeper understanding of thermo-physics and reduction of losses. EGM has been utilized in many other areas of mechanical engineering including, solar energy systems, heat exchangers, combustion, refrigeration and propulsion ducts. In the context of non-Newtonian materials processing, many studies of entropy generation have been communicated in recent years. Kumar *et al.* [18] studied the unsteady hydromagnetic flow of a Jeffrey fluid from a vertical surface using a Crank-Nicholson difference method. They showed that increasing Jeffrey fluid parameters (relaxation and retardation parameters) enhance the entropy generation number whereas the contrary effect is induced with stronger magnetic field. Srinivas and Bég [19] applied the homotopy analysis method to compute the

entropy generation in magnetized micropolar natural convection flow in a solar duct, noting that greater non-Newtonian and magnetic field effects both reduce entropy generation rates whereas the opposite behaviour is observed with increasing thermal buoyancy and dissipation effects. Opanuga *et al.* [20] used the Adomian decomposition method (ADM) to simulate entropy generation of a third-grade viscoelastic differential fluid in a channel with convective cooling in the presence of suction or injection at the walls. They found that entropy generation is enhanced by suction/injection parameter at the lower wall but reduces it at the upper wall. Reddy *et al.* [21] analysed numerically the entropy generation in time-dependent second order viscoelastic fluid convection from a vertical plate. Qayyum and Ijaz [22] conducted a second law analysis of magnetized non-Newtonian flow and heat transfer in the gap between two spinning disks using the Williamson viscoelastic model. They observed that entropy number is boosted with increasing magnetic parameter and Brinkman number whereas the Bejan number is reduced with greater magnetic parameter, Brinkman number and Weissenberg number.

The presence of high temperatures in materials operations invokes thermal radiative heat transfer. Since computational solutions of the general equation of radiative heat transfer remain challenging, most studies feature simplified radiative algebraic flux models such as the Rosseland model (diffusion approximation), P1 flux model and the Hamaker six flux model. Within the framework of boundary-layer flows, the Rosseland model remains the most popular although it is limited to fluids of high optical thickness. However, it is still appropriate for certain polymers. Shukla *et al.* [23] studied the influence of radiative flux on entropy generation in transient magnetized nano-polymer stagnation flow with chemical reaction effects. Sithole *et al.* [24] considered the impact of radiation and dissipation on entropy generation in second order electrically-conducting viscoelastic nanofluid convection from an extending sheet under a transverse magnetic field. Khan *et al.* [25] investigated the effects of Rosseland radiative parameter on mixed convection boundary layer flow of a tangent hyperbolic nanofluid with binary chemical reaction. Khan *et al.* [26] showed that radiative flux enhances temperatures and reduces entropy generation in magnetic nanofluid flow with binary chemical reaction. Murthy *et al.* [27] observed that entropy production decreases with thermal radiation in channel flow of two immiscible couple stress rheological fluids.

In recent years new sophisticated *magnetic polymers* have emerged which provide enhanced performance in many industrial sectors including aerospace, automotive, manufacturing, energy and medical engineering. These include magnetoelectric nanocomposites [28] and soft magnetic polymer gels [29]. These materials are frequently synthesized at high temperature. The current study therefore aims to simulate the *entropy*

generation minimization of transport phenomena of such materials along an inclined surface in the presence of radiative heat transfer and also dissipation effects. The objective is therefore thermodynamic optimization which is of great relevance to enhancing efficiencies of thermal coating technologies in the automotive and power industries. The Jeffrey rheological model is deployed for non-Newtonian behaviour. The emerging non-dimensional nonlinear boundary value problem is solved with the Keller box implicit finite difference method [30]. Verification of the computations is included via comparison with earlier non-magnetic studies. Extensive visualization via graphs of the influence of key parameters (Deborah viscoelastic parameter, magnetic parameter, radiative parameter, Brinkman dissipation parameter etc) on velocity, temperature, entropy generation number and Bejan number profiles is included. The present problem to the authors' knowledge has thus far not been considered in the scientific literature and constitutes a novel effort in thermodynamic analysis of magnetic non-Newtonian materials processing (coating) operations.

2. MATHEMATICAL MODEL

Natural convection in laminar, two-dimensional, time-independent incompressible Jeffrey viscoelastic magnetic polymer flow from an inclined rigid sheet is considered, as illustrated in **Fig. 1**. The sheet is inclined at an angle, Ω, to the horizontal. A static, constant-strength magnetic field is imposed externally transverse to the sheet. Uni-directional thermal radiative flux is present. The polymer is assumed to be an optically dense, absorbing but non-scattering fluent medium.

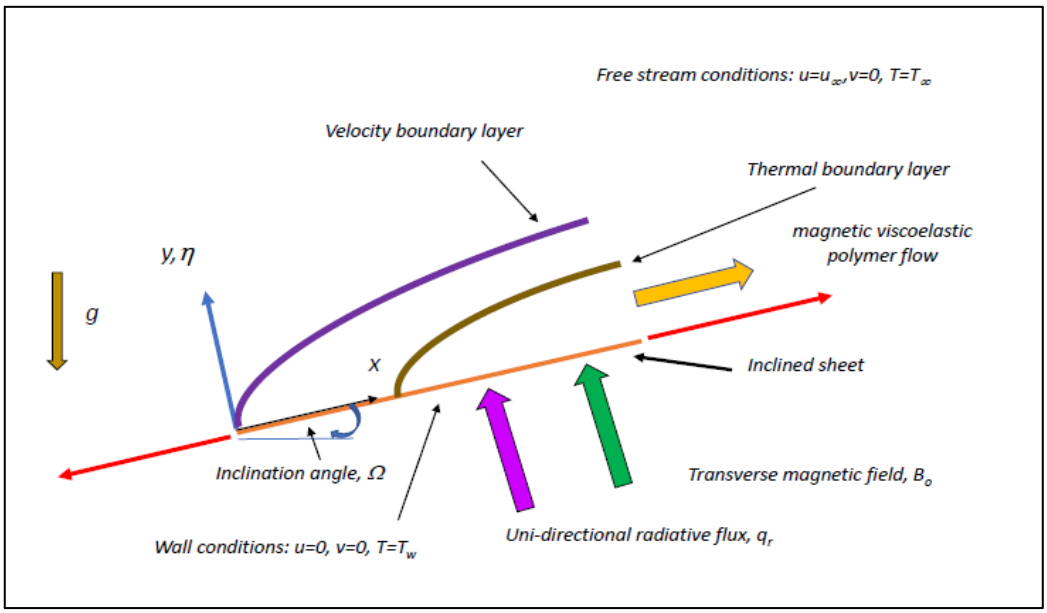

Fig 1: Physical model for radiative magnetic polymer inclined plane flow

In this model, with the exception of the density variation in the buoyancy terms (Boussinesq approximation) all other properties are assumed to be constant. To simulate non-Newtonian characteristics of the Jeffery elastic-viscous fluid model, the Cauchy stress tensor is required which is defined as [14-16, 31]:

$$T = -pI + S,\ S = \frac{\mu}{1+\lambda}\left(\dot{\gamma} + \lambda_1 \ddot{\gamma}\right) \tag{1}$$

$$\dot{\gamma} = \nabla V + \left(\nabla V\right)^t \tag{2}$$

$$\ddot{\gamma} = \frac{d}{dt}\left(\dot{\gamma}\right) \tag{3}$$

Here, p, I, S, μ, λ, λ_1 and $\dot{\gamma}$ denote pressure, identity tensor, Cauchy stress tensor for Jeffery fluid, viscosity, ratio of relaxation to retardation time, retardation time and shear rate. The Jeffery model therefore features three constants i.e. viscosity at zero shear rate, and two time-related material parameter constants. Incorporating the appropriate terms under the boundary-layer approximation, the following conservation equations emerge for mass, momentum and energy (heat):

$$\frac{\partial u}{\partial x} + \frac{\partial v}{\partial y} = 0 \tag{4}$$

$$u\frac{\partial u}{\partial x} + v\frac{\partial u}{\partial y} = \frac{\nu}{1+\lambda}\left(\frac{\partial^2 u}{\partial y^2} + \lambda_1\left(u\frac{\partial^3 u}{\partial x \partial y^2} - \frac{\partial u}{\partial x}\frac{\partial^2 u}{\partial y^2} + \frac{\partial u}{\partial y}\frac{\partial^2 u}{\partial x \partial y} + v\frac{\partial^3 u}{\partial y^3}\right)\right) + g\beta\left(T - T_\infty\right)\cos\Omega - \frac{\sigma B_0^2}{\rho}u \tag{5}$$

$$u\frac{\partial T}{\partial x} + v\frac{\partial T}{\partial y} = \frac{k}{\rho c_p}\frac{\partial^2 T}{\partial y^2} - \frac{1}{\rho c_p}\frac{\partial q_r}{\partial y} \tag{6}$$

The relevant boundary conditions imposed at the plate surface and in the free stream:

$$\begin{aligned} &\text{at} \quad y = 0, \qquad u = 0, \quad v = 0, \qquad T = T_w, \\ &\text{when} \quad y \to \infty, \quad u \to u_\infty, \quad v \to 0, \quad T \to T_\infty. \end{aligned} \tag{7}$$

The last term in the energy conservation Eq. (6) is the radiative flux term based on the Rosseland approximation. Radiative equilibrium is assumed in the simulations and the gas is also assumed to be gray. The Rosseland radiation model makes the assumption that the intensity is the black-body intensity at the fluid temperature [32]. The Rosseland model neglects the incident radiation from the extra transport equation, which saves on the computational time and uses less memory than other flux models [33]. Using this model, the flux may be written as follows:

$$q_r = \frac{4\sigma^*}{3k^*}\frac{\partial T^4}{\partial y}, \tag{8}$$

Implementing the Taylor series approximation for T^4 to express as a linear function of temperature we have following Gebhart [X]:

$$T^4 \cong 4T_\infty^3 T - 3T_\infty^4, \tag{9}$$

by using Eqs. (8)-(9) into Eq. (6), one can get:

$$u\frac{\partial T}{\partial x} + v\frac{\partial T}{\partial y} = \frac{k}{\rho c_p}\frac{\partial^2 T}{\partial y^2} + \frac{16\sigma^* T_\infty^3}{3k^*\rho c_p}\frac{\partial^2 T}{\partial y^2} \tag{10}$$

The nonlinearity of the conservation equations in primitive variables makes even a numerical solution difficult. It is judicious therefore to reduce the number of independent variables and to this end the following group of variables is invoked:

$$\begin{aligned} &\xi = \frac{x}{L}, \quad \eta = y\left(\frac{u_\infty}{\nu x}\right)^{1/2}, \quad \psi = \left(\nu u_\infty x\right)^{1/2} f, \quad De = \frac{\lambda_1 \nu \,\mathrm{Re}_x}{x^2}, \quad \mathrm{Re}_x = \frac{u_\infty x}{\nu}, \quad \mathrm{Re} = \frac{u_\infty L}{\nu} \\ &\theta(\xi,\eta) = \frac{T - T_\infty}{T_w - T_\infty}, \quad Gr = \frac{g\beta\left(T_w - T_\infty\right)L^3}{\nu^2}, \quad R = \frac{Gr}{\mathrm{Re}^2}, \quad \mathrm{Pr} = \frac{\nu\rho c_p}{k}, \quad F = \frac{K\,k^*}{4\sigma^* T_\infty^3}, \end{aligned} \tag{11}$$

Incorporating Eq. (11) into Eqs. (4), (5) and (11), the continuity equation (4) is automatically satisfied and the emerging non-dimensional momentum and thermal boundary layer equations emerge as:

$$\begin{aligned} &\frac{f'''}{1+\lambda} + \frac{1}{2}ff'' + R\xi\left(\theta + N\varphi\right)\cos\Omega - \frac{\mathrm{De}}{1+\lambda}\left(\frac{1}{2}f''^2 + f'f''' + \frac{1}{2}ff^{iv}\right) - Mf' \\ &\qquad = \xi\left(f'\frac{\partial f'}{\partial \xi} - f''\frac{\partial f}{\partial \xi} - \frac{\mathrm{De}}{1+\lambda}\left(f'\frac{\partial f'''}{\partial \xi} - f'''\frac{\partial f'}{\partial \xi} + f''\frac{\partial f''}{\partial \xi} - f^{iv}\frac{\partial f}{\partial \xi}\right)\right) \end{aligned} \tag{12}$$

$$\frac{\theta''}{\mathrm{Pr}}\left(1 + \frac{4}{3F}\right) + \frac{1}{2}f\theta' = \xi\left(f'\frac{\partial \theta}{\partial \xi} - \theta'\frac{\partial f}{\partial \xi}\right) \tag{13}$$

The transformed dimensionless wall and free stream boundary conditions assume the form:

$$\begin{aligned} &\text{at} \quad \eta = 0, \qquad f = 0, \quad f' = 0, \quad \theta = 1, \\ &\text{when} \quad \eta \to \infty, \quad f' \to 1, \quad f'' \to 0, \quad \theta \to 0, \end{aligned} \tag{14}$$

Additionally, the dimensionless expressions for the physical quantities at the plate surface can be written as:

$$\sqrt{\mathrm{Re}_x}C_f = \frac{1}{1+\lambda}\left(f''(\xi,0) - \frac{De}{2}\left(f'(\xi,0) * f''(\xi,0) + f(\xi,0) * f'''(\xi,0)\right)\right), \tag{15}$$

$$\frac{Nu}{\sqrt{\mathrm{Re}_x}} = -\theta'(\xi,0), \tag{16}$$

Here the expressions $\sqrt{\mathrm{Re}_x}\, C_f$ and $\frac{Nu}{\sqrt{\mathrm{Re}_x}}$ denote the skin friction coefficient (wall shear stress function) and the local Nusselt number (wall heat transfer rate) respectively.

3. NUMERICAL FINITE DIFFERENCE SOLUTIONS

The boundary value problem to be solved comprises Eqs. (12) and (13) under boundary conditions (14). The Keller box method is selected to obtain numerical solutions. This method is well-documented in many studies [35-37] and details are therefore omitted here. To validate the Keller box numerical code employed, comparison with earlier non-magnetic, Newtonian solutions presented by Lloyd and Sparrow [38] is conducted and shown in **Table 1**. Very close correlation is achieved for the Nusselt number (*Nu*) for different values of the mixed convection parameter (*R*) and three different values of Prandtl number (*Pr*) i.e. 0.72 (air), 10, 100 (polymers). Confidence in the present solutions is therefore very high.

Table 1: Comparison of *Nu* for different values of *R* and *Pr*

R	**Pr = 0.72**		**Pr = 10**		**Pr = 100**	
	Lloyd and Sparrow [38]	Present	Lloyd and Sparrow [38]	Present	Lloyd and Sparrow [38]	Present
0.0	0.2956	0.2955	0.7281	0.7279	1.5720	1.5719
0.01	0.2979	0.2976	0.7313	0.7310	1.5750	1.5747
0.04	0.3044	0.3042	0.7404	0.7402	1.5850	1.5848
0.1	0.3158	0.3155	0.7574	0.7571	1.6050	1.6049
0.4	0.3561	0.3557	0.8259	0.8255	1.6910	1.6905
1.0	0.4058	0.4054	0.9212	0.9209	1.8260	1.8258

4. ENTROPY GENERATION ANALYSIS

The entropy generation analysis for the present flow regime is now described, following Bejan [38]. The volumetric rate of entropy generation due to magnetic field with heat transfer is given as:

$$S'''_{gen} = \frac{k}{T_\infty^2}\left(\frac{\partial T}{\partial y}\right)^2 + \frac{\mu}{T_\infty}\left(\frac{\partial u}{\partial y}\right)^2 + \frac{\sigma B_0^2 u^2}{T_\infty} \qquad (17)$$

The first term in eq. (17) signifies the entropy generation produced by *heat flow*, the second term denotes the entropy generation due to *viscous dissipation* and the final term is the entropy

generation due to the *magnetic Lorentz force*. The dimensionless *entropy heat generation* (N_G) is the ratio of the *volumetric rate of entropy generation* to the *characteristic entropy heat generation rate*.

$$N_G = \frac{S'''_{gen}}{S''_0} = \left(\frac{\frac{k}{T_\infty^2}\left(\frac{\partial T}{\partial y}\right)^2 + \frac{\mu}{T_\infty}\left(\frac{\partial u}{\partial y}\right)^2 + \frac{\sigma B_0^2 u^2}{T_\infty}}{\frac{k(\Delta T)^2}{l^2 T_\infty^2}} \right) \tag{18}$$

$$N_G = \mathrm{Re}\,\theta'^2 + \frac{Br}{\Omega}\mathrm{Re}\, f''^2 + \frac{Br}{\Omega} Ha^2 f'^2 \tag{19}$$

Here $\mathrm{Re} = \frac{l^2 Gr^{1/2}}{a^2}$, $Br = \frac{\mu u^2}{k\Delta T}$, $M = Ha = B_0 l\sqrt{\frac{\sigma}{\mu}}$, $\Omega = \frac{\Delta T}{T_\infty}$ and $u = \frac{\nu Gr^{1/2}}{a^2}\xi$. Eq. (19) can be written as, $N_G = N_1 + N_2$. Furthermore, $N_1 = \mathrm{Re}\,\theta'^2$ and $N_2 = \frac{Br}{\Omega}\mathrm{Re}\, f''^2 + \frac{Br}{\Omega} Ha^2 f'^2$ are the irreversibility owing to heat transfer and viscous dissipation respectively. The irreversibility distribution is defined via the *Bejan number* (*Be*) which is defined as the ratio of entropy heat generation due to heat transfer to the overall entropy heat generation i.e.:

$$Be = \frac{N_1}{N_G} \tag{20}$$

Bejan number, *Be* lies between 0 and 1 *i.e,* $0 \le Be \le 1$. Therefore, if $Be = 0$, N_2 dominates N_1 and vice versa if $Be = 1$. Furthermore, when $Be = 0.5$, the fluid friction contribution in entropy generation and the irreversibility due to heat transfer are equal *i.e.*, $N_1 = N_2$.

5. RESULTS AND DISCUSSION

Figs 2–25 illustrate graphical solutions for the influence of selected parameters on the velocity, temperature and entropy characteristics. In all graphs plate inclination is set at $\Omega = \pi/6$. Asymptotically smooth distributions are generally achieved in the freestream for all graphs indicating that a sufficiently large infinity boundary condition is specified in the Keller box numerical code.

Rheological effects

Figs. 2 – 5 depict the influence of Deborah number (viscoelastic parameter) on velocity, temperature, entropy generation number and Bejan number (f', θ, Ng and Be). **Fig. 2** shows the influence of De on f' and clearly increasing *De* (which corresponds to greater elastic effects to viscous effects) results in flow acceleration. *De* embodies the ratio of the relaxation

time characterizing the time it takes for the fluid to adjust to applied stresses or deformations, and the characteristic time scale. Momentum boundary layer thickness is therefore reduced with increasing Deborah number. The fluid (polymer) behaves more like a viscous fluid at lower Deborah number whereas at higher Deborah numbers, the behaviour is more influenced by elasticity. **Fig. 3** demonstrates that increasing *De* values also result in a decrease in temperature i.e. reduction in thermal boundary layer thickness. The effect of *De* on the entropy generation number is shown in **Fig. 4** and it is apparent that an increase in entropy generation occurs initially. However further from the plate surface there is a depression in entropy generation with increasing *De*. **Fig. 5** shows that an increase in *De* generally reduces the Bejan number (*Be*).

Figs. 6 – 9 show the response in fluid velocity (f'), temperature (θ), entropy generation number (Ng) and Bejan number (Be) with ratio of relaxation to retardation times (λ). A significant elevation in velocity accompanies an increase in λ as observed in Fig. 6. Conversely, there is a strong reduction in temperature with increasing λ values (Fig. 7). Entropy generation number (Ng) is strongly reduced with increasing λ values close to the plate surface (Fig. 8). However, further from the plate towards the free stream of the boundary layer this trend is reversed and evidently *Ng* values are found to be enhanced with increasing λ values. Fig. 9 shows that Bejan number is substantially reduced with increasing values of the ratio of relaxation to retardation times (λ). Effectively therefore the rheology of the Jeffery fluid has a marked influence on thermal and hydrodynamic characteristics. For the case of a Newtonian fluid ($\lambda = 1$), the results are noticeably different from the Jeffery case ($\lambda \neq 1$). When $\lambda_1 < 1$ the retardation time exceeds the relaxation time. This implies that the polymeric Jeffrey fluid responds faster with the removal of stress and returns quicker to its unperturbed state. The opposite behaviour is the case when $\lambda_1 > 1$.

Mixed convection effects

Figs. 10 – 13 visualize the response in fluid velocity (f'), Jeffery fluid temperature (θ), entropy generation number (Ng) and Bejan number (Be) to a variation in *mixed convection parameter* (*R*). Larger values of *R* correspond to stronger natural (free) convection *i.e*. greater Grashof numbers. A significant elevation in velocity is induced throughout the boundary layer transverse to the plate surface with increasing mixed convection parameter, *R*, as seen in Fig. 10. Momentum boundary layer thickness is therefore decreased. Temperatures are considerably depleted (Fig. 11) with greater *R* values *i.e*. thermal boundary layer thickness is reduced. In both Figs. 10 and 11 the trends are sustained throughout the boundary layer. Fig.

12 shows that in close proximity to the plate surface there is an enhancement in the entropy generation number with a rise in mixed convection parameter, whereas further from the plate there is a decrease. Furthermore, for $\eta > 4.1$ the entropy generation number asymptotically converges to zero. Bejan number (Fig. 13) is dramatically reduced both close to and far from the plate with increasing mixed convection parameter. However, at intermediate distance from the plate surface all Bejan number profiles converge indicating that in this region there is no tangible influence of the mixed convection.

Radiative heat transfer effects

Figs. 14 – 17 show the distributions for velocity (f'), fluid temperature (θ), entropy generation number (Ng), and Bejan number (Be) with different values of thermal radiation parameter (F). Fig. 14 indicates that a weak acceleration in the boundary layer flow is associated with a large rise in radiation parameter, F (values are increased from 0.01 to 1.5). Increasing thermal radiation parameter (F) is observed in Fig. 15 to strongly elevate the fluid temperature (θ). Radiative flux energizes the boundary layer flow and augments the thermal diffusivity. This enhances temperatures and increases thermal boundary layer thickness. Fig. 16 shows that entropy generation number (Ng) declines significantly for the range of $0 \leq \eta \leq 1.6$ (near the plate surface) with increasing radiation parameter values. However further from the plate surface the contrary behaviour is computed and there is a reduction in entropy generation number. Minimum entropy production is therefore obtained further from the plate surface. Fig. 17 reveals that close to the plate surface there is a strong decrease in Bejan number with increasing radiative parameter whereas the reverse behaviour is observed further from the plate surface. At the plate surface Bejan number is minimized. This represents the dominance of fluid friction at the plate. The entropy generation will be increased when the temperature and velocity gradients are high. Therefore, the increase in these gradients leads to an increase in the irreversibility in the flow.

Magnetohydrodynamic effects

Figs. 18 – 21 depict the evolution in velocity (f'), Jeffery fluid temperature (θ), entropy generation number (Ng) and Bejan number (Be) with a modification in magnetic field parameter (M). Fig 18 shows that increasing magnetic effect depletes the velocity magnitudes. Increasing the values of magnetic parameter result in an increase in the Lorentzian magnetohydrodynamic drag force. This decreases the friction (shearing effect) at the plate surface and this effectively reduces the flow velocity. Stronger applied magnetic field opposes the momentum transport i.e. induces flow deceleration and therefore increases momentum

boundary layer thickness. Conversely temperature (Fig. 19) is strongly elevated with increasing magnetic field effect. The supplementary work expended by dragging the Jeffery fluid against the action of the magnetic field is dissipated as thermal energy i.e. heat. This elevates temperatures in the boundary layer regime and increases thermal boundary layer thickness. Fig. 20 shows that a substantial plummet in entropy generation number is generated with a rise in magnetic parameter. The converse response is induced in Bejan number (Fig. 21) which is markedly elevated with increasing magnetic field and this is consistent throughout the boundary layer regime.

Reynolds number effects

Figs. 22 – 23 illustrate the distributions in **e**ntropy generation number (Ng) and Bejan number (Be) with a range of Reynolds numbers (Re).Both the entropy generation number and Bejan number are increasing function of *Re* although the former is modified more dramatically closer to the plate than the latter and vice versa further from the plate over the same increment in Reynolds numbers. Evidently with greater inertial and lesser viscous effect entropy generation is encouraged in the boundary layer flow.

Viscous dissipation effects

Figs 24 – 25 depict the impact of Brinkmann (Br) on both the entropy generation number (Ng) and Bejan number (Be). It is evident from Fig. 24 that with increasing Br (= 1, 1.5, 2, 2.5, 3, 3.5) the entropy generation number is greatly boosted in magnitude and the effect is most prominent near the plate surface. Brinkman number is related to the heat conduction from the wall to the viscous fluid and characterizes the viscous dissipation term in the fluid flow. With increasing Brinkman number, the thermal conductivity of the fluid decreases so a greater quantity of heat can be transferred through the fluid. This manifests in an elevation in entropy generation. Conversely the Bejan number (Fig. 25) is observed to be decreased with increasing Brinkman number particularly near the plate and for some distance into the boundary layer, thereafter converging quickly towards zero.

6. CONCLUSIONS

A mathematical model has been developed to simulate the entropy generation in steady-state natural convection boundary layer flow of an electrically-conducting dissipative viscoelastic fluid (magnetic polymer) from an inclined plate in the presence of thermal radiation. The governing conservation equations for mass, momentum and energy and

associated wall and free stream boundary conditions have been transformed to a nonlinear dimensionless boundary value problem. The Jeffery elastic-viscous model has been used. The model has been developed to simulate magnetic non-Newtonian materials processing. An implicit finite difference scheme (Keller box method) has been implemented to solve the partial differential boundary value problem computationally. Bejan's entropy generation minimization approach has been adopted to conduct a second law thermodynamic analysis of the flow. The main conclusions from the present study may be summarized as follows:

- Velocity is enhanced with increasing Deborah number, relaxation to retardation ratio, mixed convection parameter and Reynolds number whereas it is decreased with increasing magnetic field parameter.
- Temperature is reduced with increasing Deborah number, relaxation to retardation ratio, mixed convection parameter whereas it is strongly elevated with increasing radiation parameter and magnetic parameter.
- Entropy generation number is generally boosted with increasing Deborah number, relaxation to retardation ratio, mixed convection parameter, Reynolds number and Brinkman (dissipation) number whereas it is decreased with increasing radiative and magnetic parameters.
- Bejan number is an increasing function of magnetic field parameter and Reynolds number whereas it is a decreasing function of Deborah number, relaxation to retardation ratio, mixed convection parameter, radiation parameter and Brinkman number.

The present study has ignored transient effects. These will be considered in the future in addition to alternative rheological models e.g. Oldroyd-B fluid model [39], which is also relevant to thermal polymer processing.

REFERENCES

[1] Huang, X. and Gollner M.J., Correlations for evaluation of flame spread over an inclined fuel surface. *Fire Safety Science,* 11, 222-233 (2014).

[2] P. Cheng, Film condensation along an inclined surface in a porous medium, *International Journal of Heat and Mass Transfer,* 24, 983-990 (1981).

[3] O. Anwar Bég, J. Zueco and T.B. Chang, Numerical analysis of hydromagnetic gravity-driven thin film micropolar flow along an inclined plane, *Chemical Engineering Communications,* 198, 3, 312- 331 (2010).

[4] N.J. Balmforth *et al.,* Viscoplastic flow over an inclined surface, *J. Non-Newtonian Fluid Mechanics,* 142, 219-243 (2007).

[5] M.B. Ashraf *et al.,* Radiative mixed convection flow of an Oldroyd-B fluid over an inclined stretching surface, *Journal of Applied Mechanics and Technical Physics*, 57, 317–325 (2016).

[6] Pruess, K., Zhang, Y., A hybrid semi-analytical and numerical method for modeling wellbore heat transmission, *Proc. 30th Workshop on Geothermal Reservoir Engineering, Stanford University, Stanford, California, USA* (2005).

[7] Y. Greener and S. Middleman, Blade-coating of a viscoelastic fluid, *Polymer Engineering and Science,* 14, 791-796 (1974).

[8] H.-C. Chang and E. A. Demekhin, *Complex Wave Dynamics on Thin Films,* Elsevier, Amsterdam (2002).

[9] A.F. Johnson, Rheology of thermoplastic composites I, *Composites Manufacturing*, 6, 153-160 (1995).

[10] J. Sui *et al.,* Convection heat transfer of power-law fluids along the inclined nonuniformly heated plate with suction or injection, *ASME J. Heat Transfer.* 138(2):021701-021701-8 (2015).

[11] M.D. Shamshuddin, S.R. Mishra, O. Anwar Bég and A. Kadir, Unsteady reactive magnetic radiative micropolar flow, heat and mass transfer from an inclined plate with Joule heating: a *model for magnetic polymer processing, Proc. IMechE- Part C. – Mechanical Engineering Science* (2018). DOI: 10.1177/0954406218768837 (16 pages)

[12] M. Helal and M.A. Saif, Free convection heat and mass transfer in a power law fluid past an inclined surface with thermophoresis, *J. Egyptian Mathematical Society*, 21, 224-232 (2013).

[13] T. Chinyoka *et al.*, Computational analysis of gravity driven flow of a variable viscosity viscoelastic fluid down an inclined plane, *Computers & Fluids,* 84, 1-10 (2013).

[14] N. Manzoor, K. Maqbool, O. Anwar Bég and S. Shaheen, Adomian decomposition solution for propulsion of dissipative magnetic Jeffrey biofluid in a ciliated channel containing a porous medium with forced convection heat transfer, *Heat Transfer - Asian Research* (2018). DOI: 10.1002/htj.21394

[15] V.R. Prasad, S. Abdul Gaffar, E. Keshava Reddy and O. Anwar Bég, Numerical study of non-Newtonian boundary layer flow of Jeffreys fluid past a vertical porous plate in a non-Darcy porous medium, *Int. J. Comp. Meth. Engineering Science & Mechanics,* 15 (4) 372-389 (2014).

[16] S. Abdul Gaffar, V. Ramachandra Prasad, O. Anwar Bég, Md. Hidayathullah Khan, K. Venkatadri, Effects of ramped wall temperature and concentration on viscoelastic Jeffrey's fluid flows from a vertical permeable cone, *J. Brazilian Soc. Mech Sci. Eng.* 40, 441-459 (2018).

[17] Bejan, A.: The concept of irreversibility in heat exchanger design: counter flow heat exchangers for gas-to-gas applications, *ASME Journal of Heat Transfer* 99, 374-380 (1977).

[18] M. Kumar, G.J. Reddy and N. Dalir, Transient entropy analysis of the magnetohydrodynamics flow of a Jeffrey fluid past an isothermal vertical flat plate, *Pramana,* 91:60 (2018).

[19] J. Srinivas and O. Anwar Bég, Homotopy study of entropy generation in magnetized micropolar flow in a vertical parallel plate channel with buoyancy effect, *Heat Transfer Research,* 49(6): 529–553 (2018).

[20] A. A. Opanuga *et al.,* Effect of suction/injection on the entropy generation of third grade fluid with convective cooling, *Defect and Diffusion Forum*, 384, 21-30 (2018).

[21] G. J. Reddy, M. Kumar and O. Anwar Bég, Effect of temperature dependent viscosity on entropy generation in transient viscoelastic polymeric fluid flow from an isothermal vertical plate, *Physica A - Statistical Mechanics and its Applications,* 510, 426–445 (2018).

[22] S. Qayyum, M. Ijaz Khan, T. Hayat, A. Alsaedi, M. Tamoor, Entropy generation in dissipative flow of Williamson fluid between two rotating disks, *International Journal of Heat and Mass Transfer*, 127, 933-942 (2018).

[23] N. Shukla, Puneet Rana, O. Anwar Bég, A. Kadir and Bani Singh, Unsteady electromagnetic radiative nanofluid stagnation-point flow from a stretching sheet with chemically reactive nanoparticles, Stefan blowing effect and entropy generation, *Proc. IMechE: Part N-Journal of Nanomaterials, Nanoengineering and Nanosystems (2018). DOI: 10.1177/2397791418782030 (14 pages)*

[24] H. Sithole, Hiranmoy Mondal, Precious Sibanda, Entropy generation in a second grade magnetohydrodynamic nanofluid flow over a convectively heated stretching sheet with nonlinear thermal radiation and viscous dissipation, *Results in Physics*, 9, 1077-1085 (2018).

[25] M. Ijaz Khan, Sumaira Qayyum, T. Hayat, M. Imran Khan, A. Alsaedi, Tufail Ahmad Khan, Entropy generation in radiative motion of tangent hyperbolic nanofluid in presence of activation energy and nonlinear mixed convection, *Physics Letters A*, 382, 2017-2026 (2018).

[26] Muhammad Ijaz Khan, Sumaira Qayyum, Tasawar Hayat, Muhammad Waqas, Muhammad ImranKhan, Ahmed Alsaedi, Entropy generation minimization and binary

chemical reaction with Arrhenius activation energy in MHD radiative flow of nanomaterial, *J. Mol. Liq.*, 259, 274-283 (2018).

[27] J. V. Ramana Murthy, J. Srinivas and O. Anwar Bég, Entropy generation analysis of radiative heat transfer effects on channel flow of two immiscible couple stress fluids, *J. Brazilian Soc. Mech Sci. Eng*, 39, 2191–2202 (2017).

[28] A. Maceiras and P. Martins, High-temperature polymer based magnetoelectric nanocomposites, *European Polymer Journal*, 64, 224-228 (2015).

[29] P.M. Xulu, P. Filipcsei, M. Zrinyi, Preparation and responsive properties of magnetically soft poly(*N*-isopropylacrylamide) gels, *Macromolecules*, 33 (5) 1716-1719 (2000).

[30] O. Anwar Bég, Numerical methods for multi-physical magnetohydrodynamics, Chapter 1, pp. 1-112, *New Developments in Hydrodynamics Research, M. J. Ibragimov and M. A. Anisimov, Eds., Nova Science, New York, September* (2012).

[31] M.T. Shaw, *Introduction to Polymer Rheology*, Wiley, New York (2012).

[32] Modest, M.F, *Radiative Heat Transfer*, Third edition, Acad. Press, New York (2013).

[33] Gebhart, B.,

[33] O. Anwar Bég, S. Kuharat, R. Mehmood, R. Tabassum and M. Babaie, Oblique radiative solar nano-polymer gel coating heat transfer and slip flow: manufacturing simulation, *ICHTFM 2018: 20th Int. Conf. Heat Transfer & Fluid Mechanics***,** *Istanbul, Turkey, August 16-17* (2018).

[34] S. Abdul Gaffar, O. Anwar Bég, V. R. Prasad, Mathematical modelling of natural convection in a third grade viscoelastic micropolar fluid from an isothermal inverted cone, *Iran J Sci Technol. Trans Mech Eng (2018) DOI 10.1007/s40997-018-0262-x (21 pages)*

[35] A. Subba Rao, Prasad, V.R., O. Anwar Bég, Rashidi, M., Free convection heat and mass transfer of a nanofluid past a horizontal cylinder embedded in a non-Darcy porous medium, *J. Porous Media*, 21 (3), 279-294 (2018).

[36] B. Vasu, Rama S. R. Gorla, O. Anwar Bég, P. V. S. N. Murthy, V. R. Prasad and A. Kadir, Unsteady flow of a nanofluid over a sphere with non-linear Boussinesq approximation, *AIAA J. Thermophysics Heat Transfer (2018). 13 pages. DOI: 10.2514/1.T5516*

[37] S. A. Gaffar, V. R. Prasad, B. R. Kumar and O. Anwar Bég, Computational modelling and solutions for mixed convection boundary layer flows of nanofluid from a non-isothermal wedge, *J. Nanofluids*, 7, 1–9 (2018).

[38] Lloyd JR, Sparrow EM. Combined forced and free convection flow on vertical surfaces. *International Journal Heat Mass Transfer*, 13(2), 434-438 (1970).

[39] M. Norouzi, M. Davoodi and O. Anwar Bég, MD. Shamshuddin, Theoretical study of Oldroyd-B visco-elastic fluid flow through curved pipes with slip effects in polymer flow

processing, *Int. J. Applied Computational Mathematics https://doi.org/10.1007/s40819-018-0541-7 (22 pages)*

FIGURES

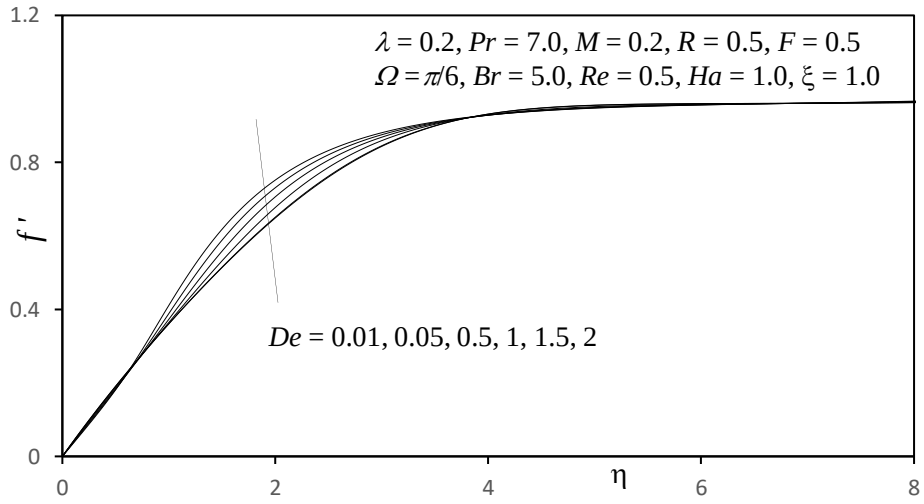

Fig. 2 Influence of *De* on Velocity Profiles

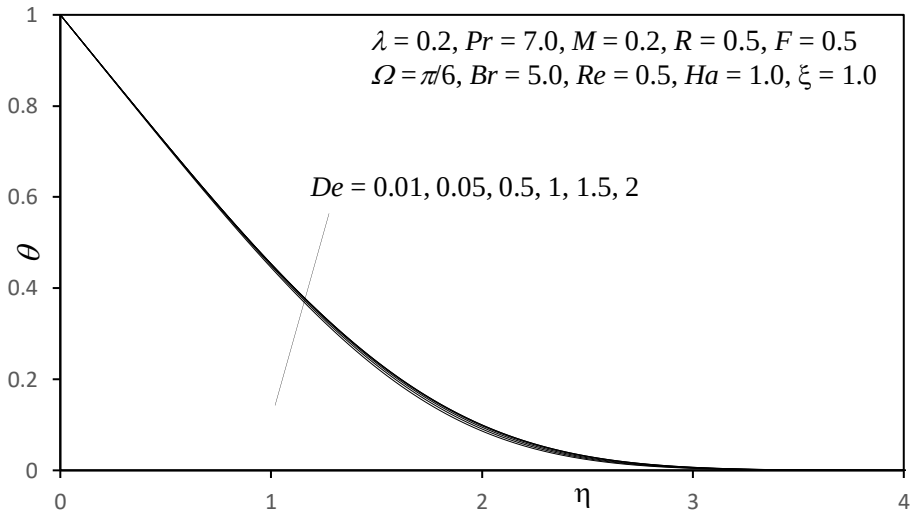

Fig. 3 Influence of *De* on Temperature Profiles

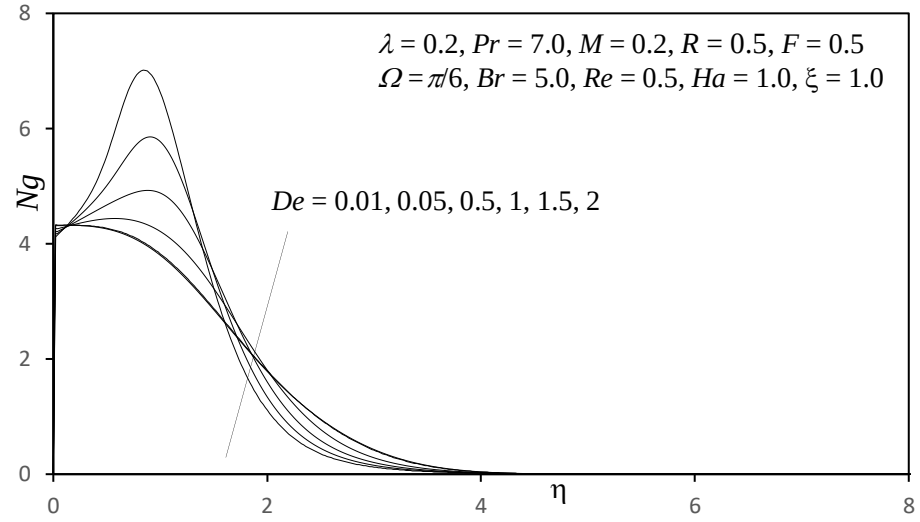

Fig. 4 Influence of *De* on Entropy Generation number

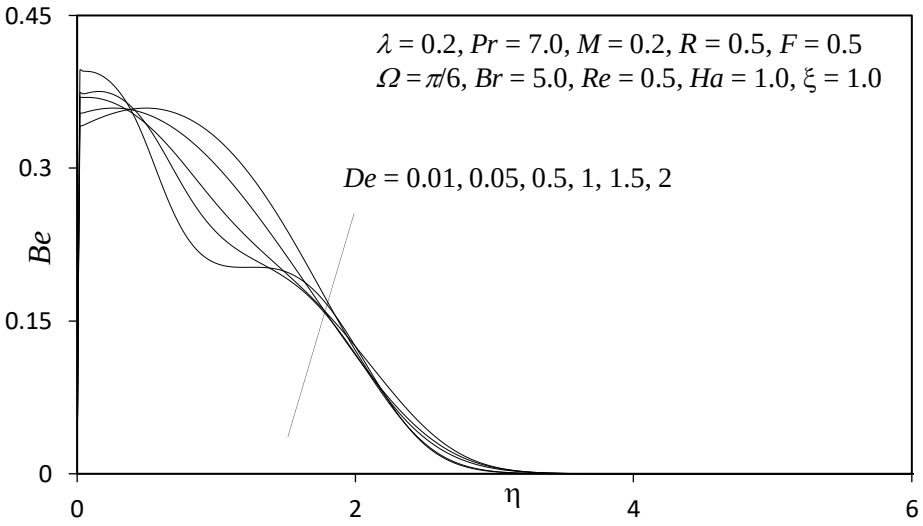

Fig. 5 Influence of *De* on Bejan number

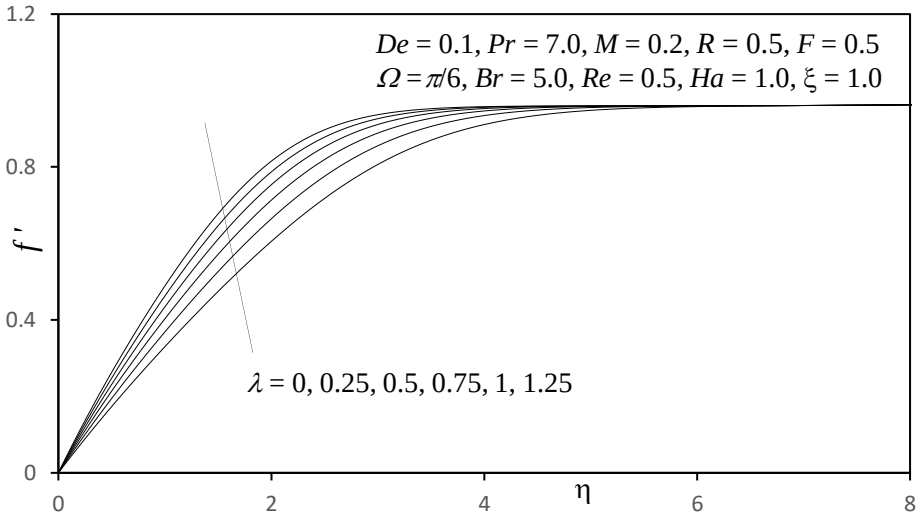

Fig.6 Influence of λ on Velocity Profiles

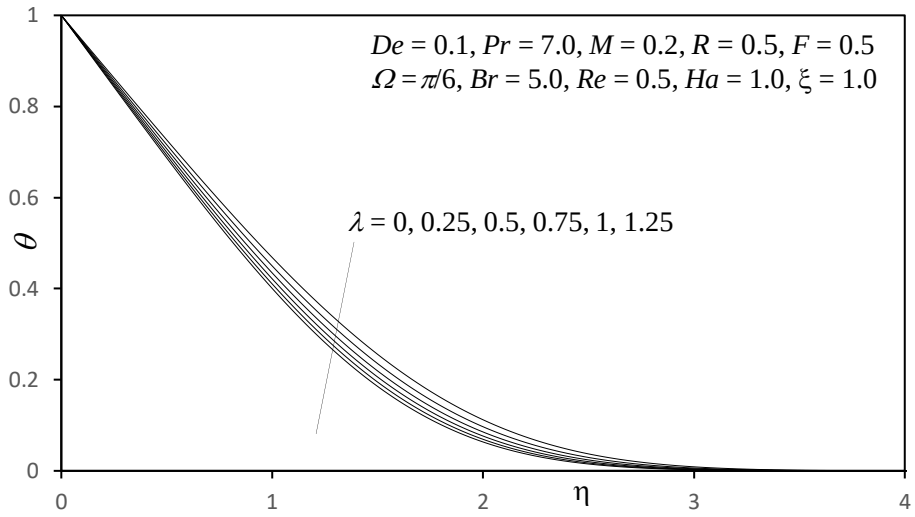

Fig. 7 Influence of λ on Temperature Profiles

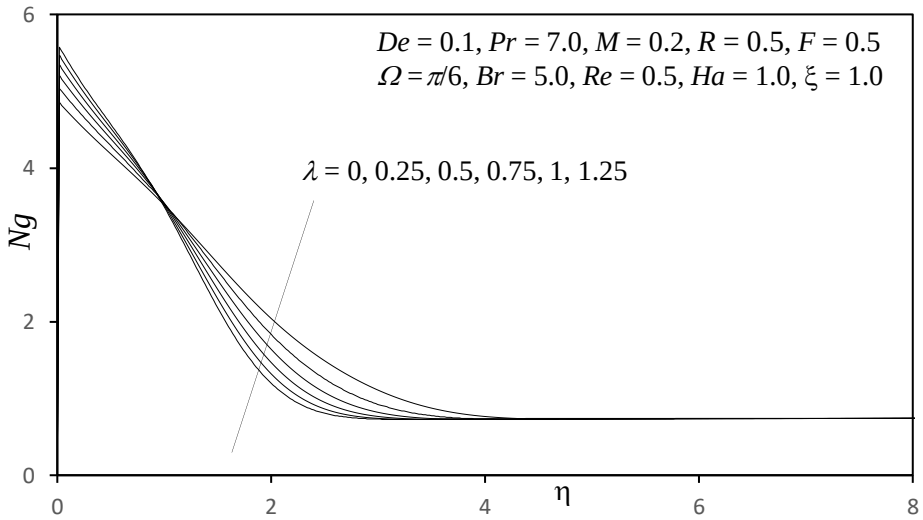

Fig. 8 Influence of λ on Entropy Generation number

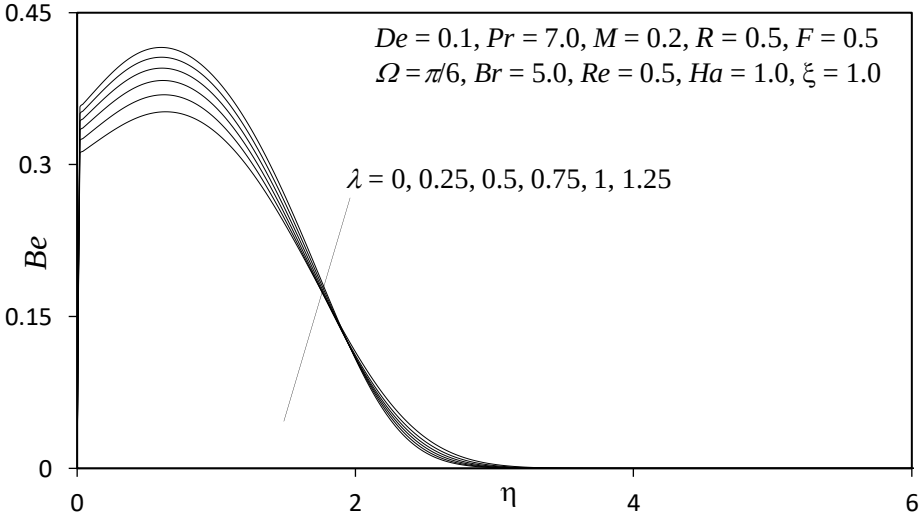

Fig. 9 Influence of λ on Bejan number

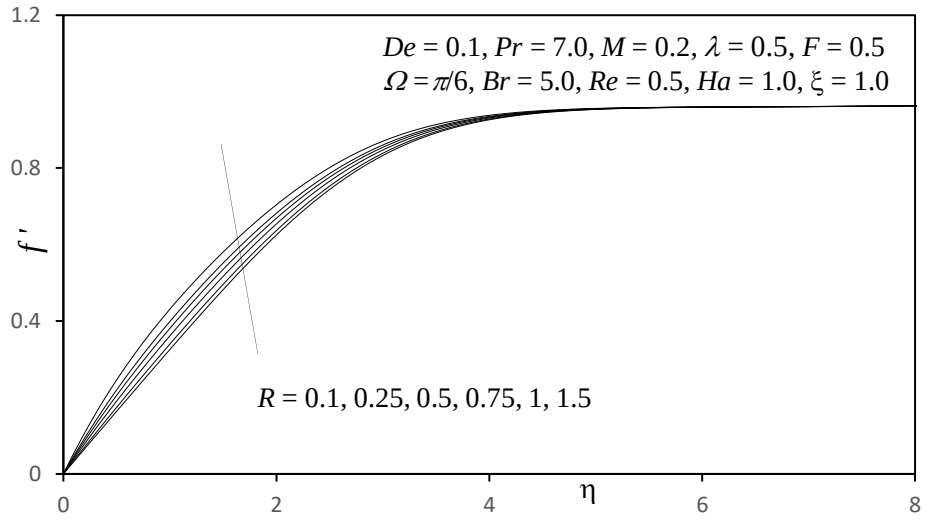

Fig. 10 Influence of *R* on Velocity Profiles

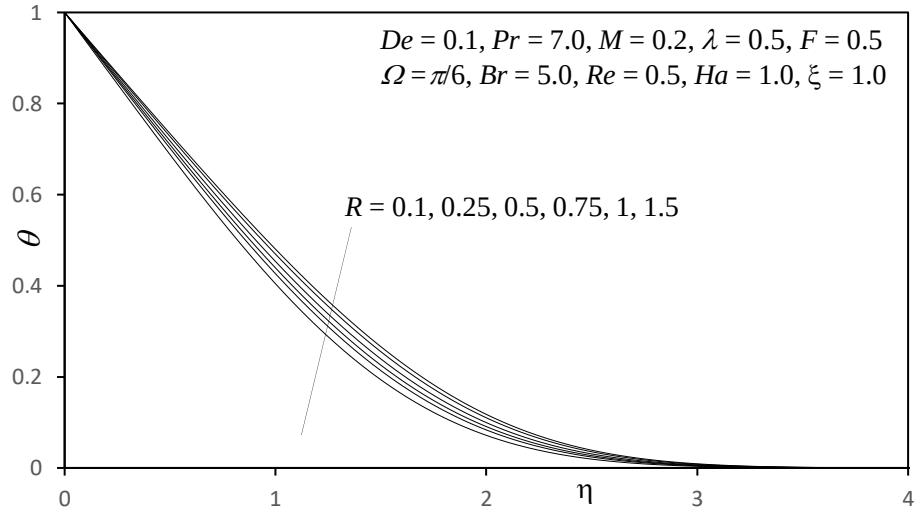

Fig. 11 Influence of *R* on Temperature Profiles

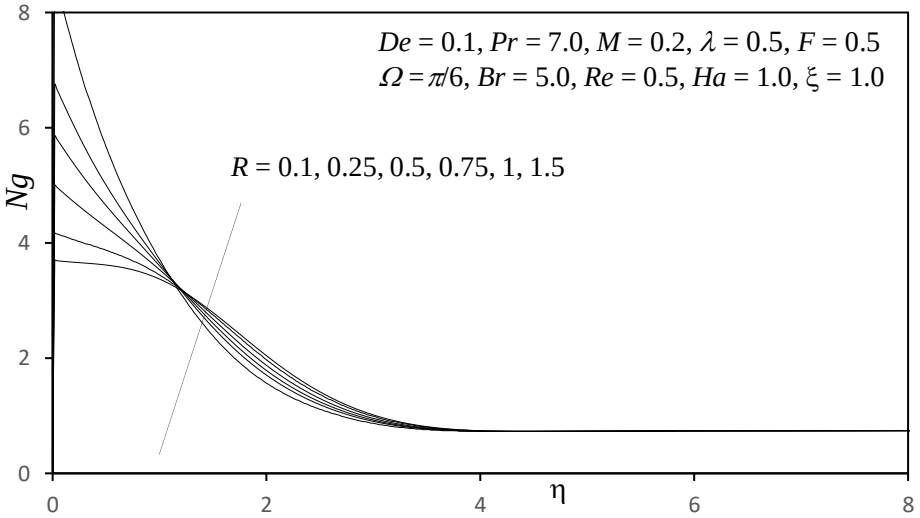

Fig. 12 Influence of *R* on Entropy Generation number

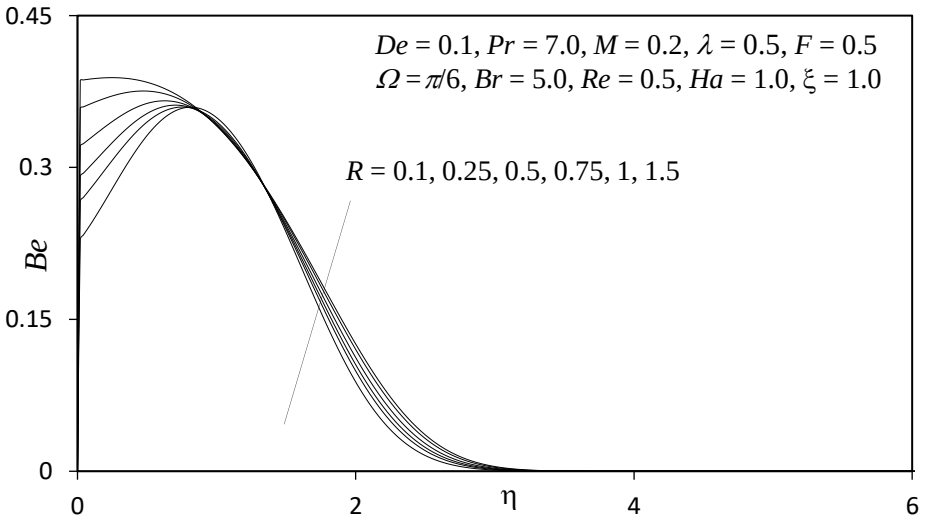

Fig. 13 Influence of R on Bejan number

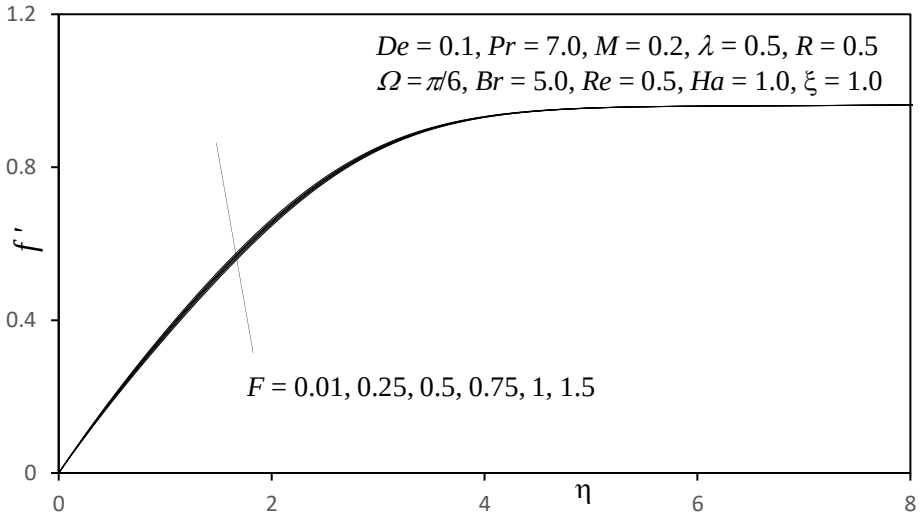

Fig. 14 Influence of F on Velocity Profiles

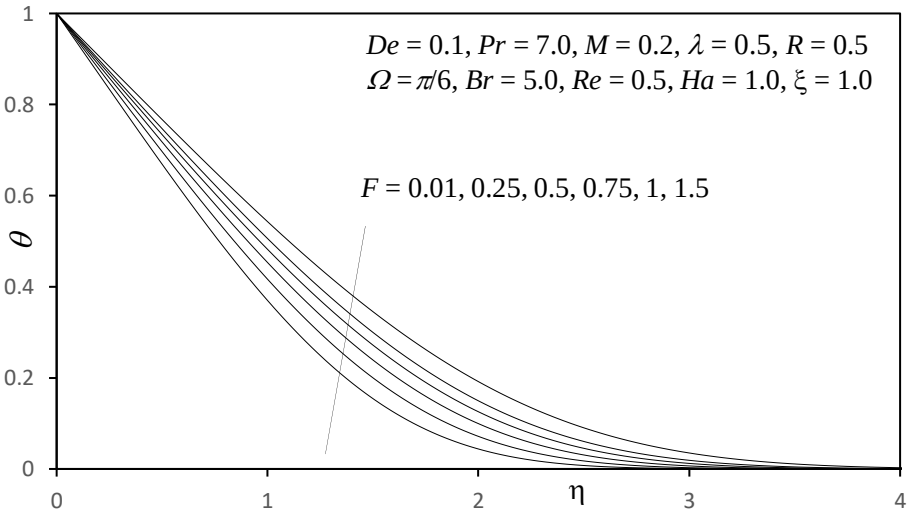

Fig. 15 Influence of F on Temperature Profiles

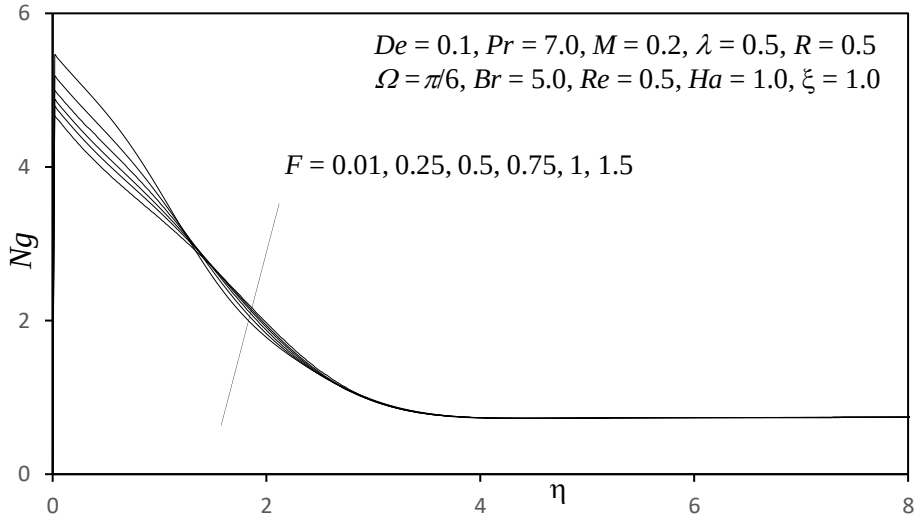

Fig. 16 Influence of *F* on Entropy Generation number

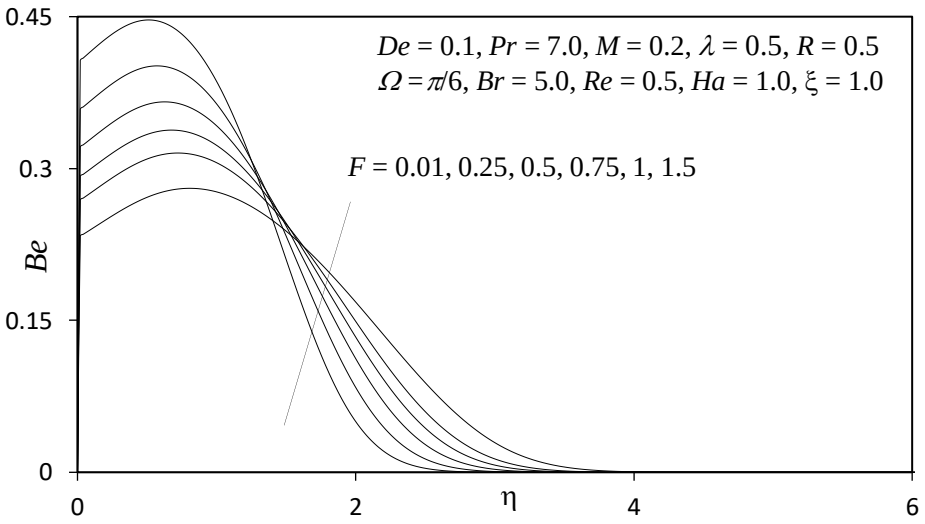

Fig. 17 Influence of *F* on Bejan number

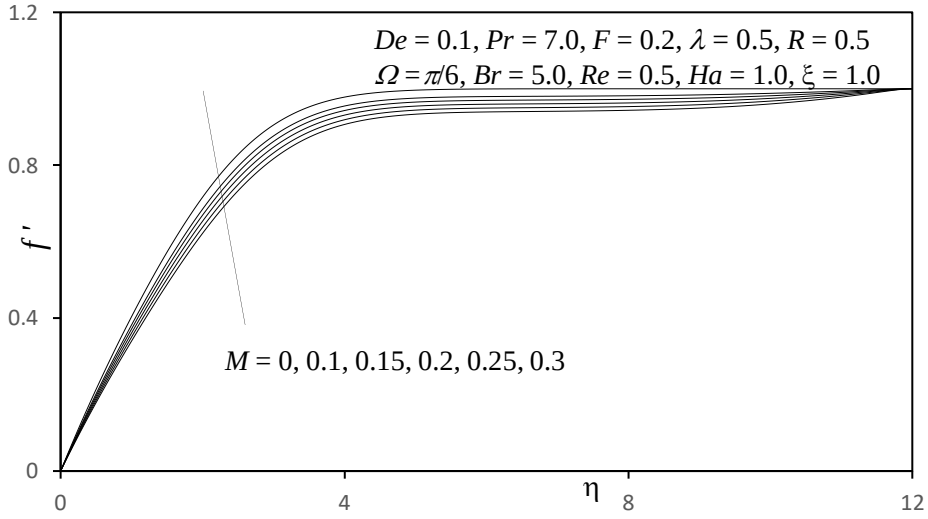

Fig. 18 Influence of *M* on Velocity Profiles

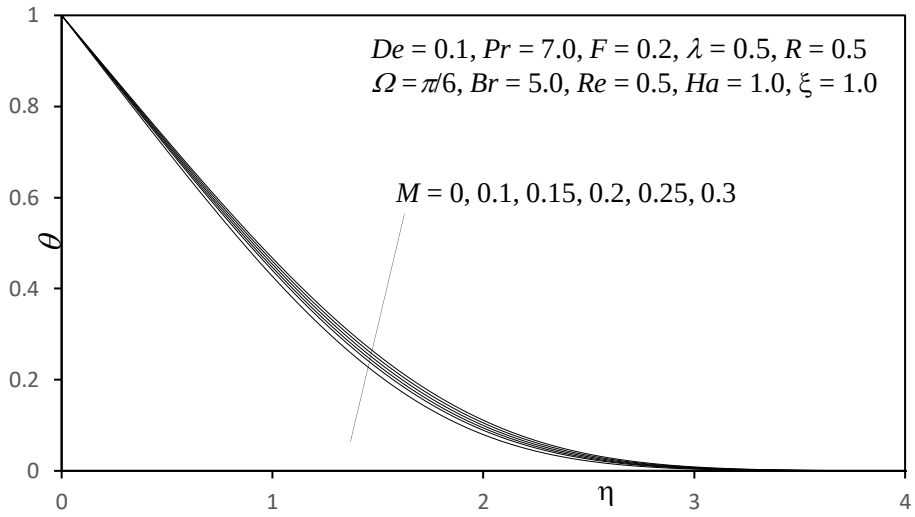

Fig. 19 Influence of *M* on Temperature Profiles

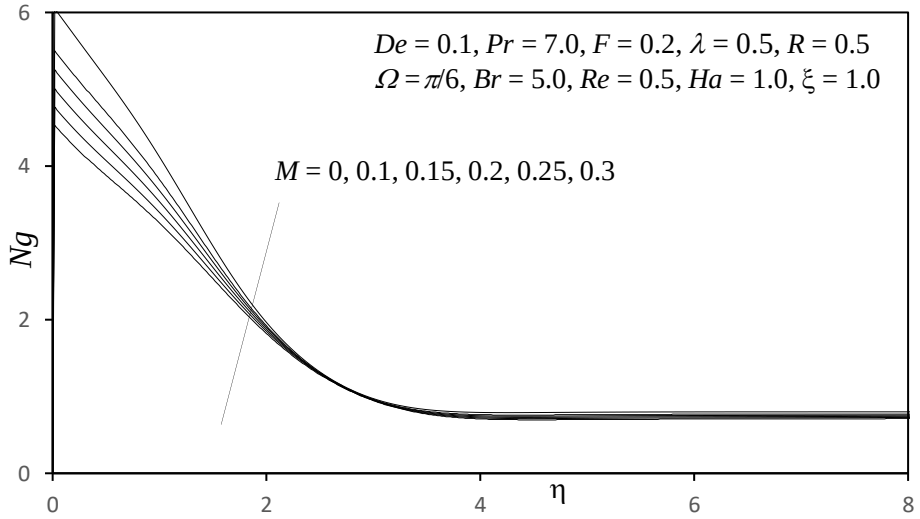

Fig. 20 Influence of *M* on Entropy Generation number

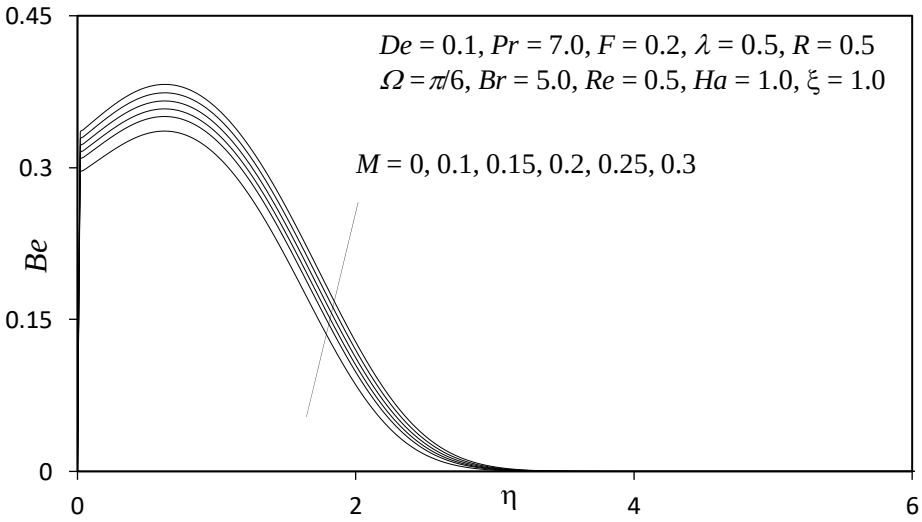

Fig. 21 Influence of *M* on Bejan number

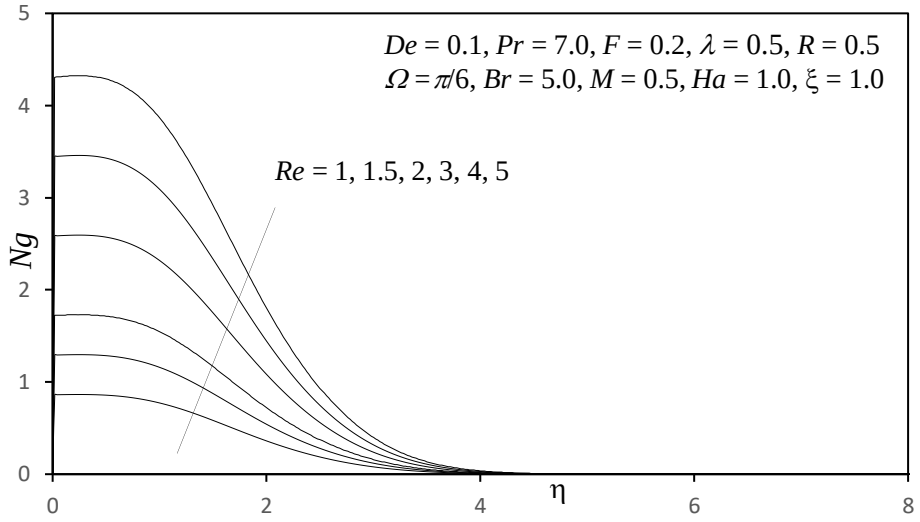

Fig. 22 Influence of *Re* on Entropy Generation number

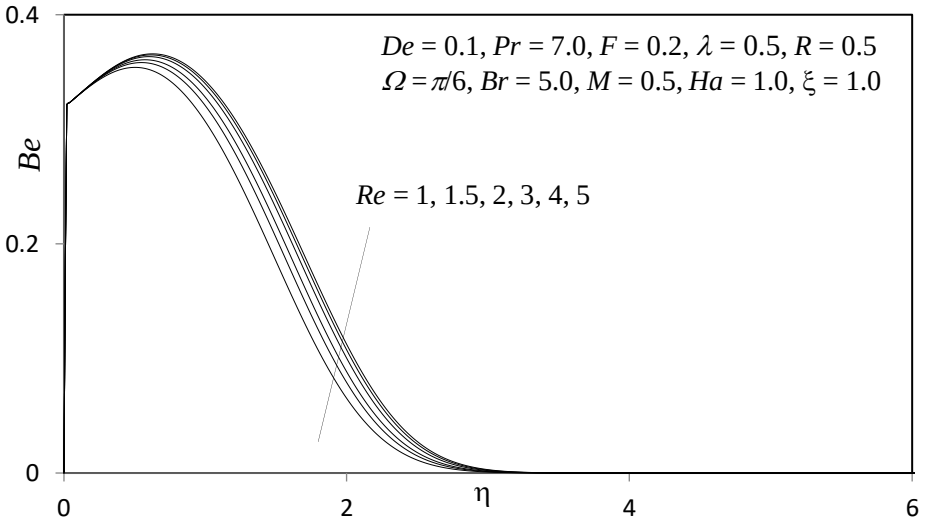

Fig. 23 Influence of *Re* on Bejan number

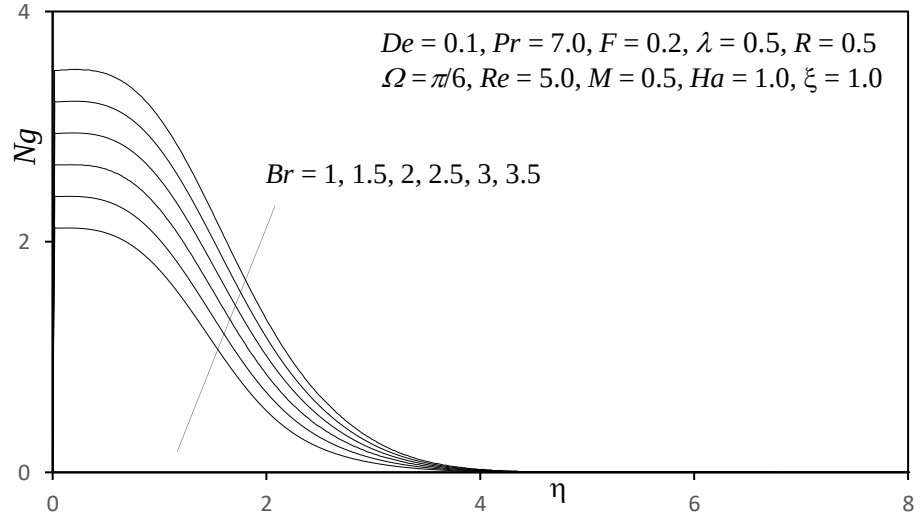

Fig. 24 Influence of *Br* on Entropy Generation number

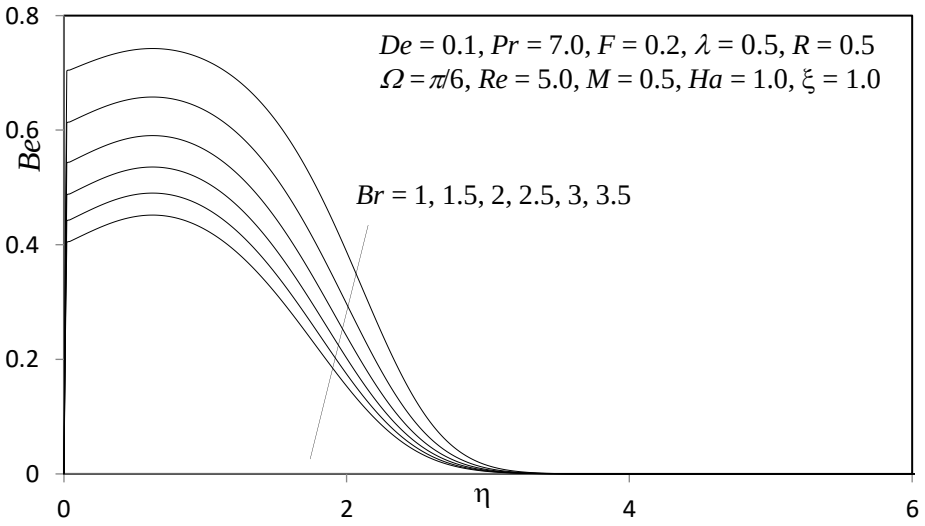

Fig. 25 Influence of *Br* on Bejan number